Block Copolymer Encapsulation of Disarib, an Inhibitor of BCL2 for Improved Chemotherapeutic Potential

Reshma Joy, Humaira Siddiqua, Shivangi Sharma, Manthra Raveendran, Franklin John, Puthusserickal Abdulrahiman Hassan, Santosh L Gawali, Sathees C. Raghavan, and Jinu George*

Read Online

ACCESS | Metrics & More | Article Recommendations

ABSTRACT: A chemical inhibitor of antiapoptotic protein, BCL2, known as Disarib, suffers poor solubility in aqueous environments; thereby limiting its potential as a chemotherapeutic agent. To overcome this limitation and enhance the therapeutic efficacy of Disarib, we have employed the encapsulation of this small molecule inhibitor within P123 copolymer matrix. Micelles were synthesized using a thin-film hydration technique, and a comprehensive analysis was undertaken to evaluate the resulting micelle properties, including morphology, particle size, intermolecular interactions, encapsulation efficiency, and *in vitro* release characteristics. This assessment utilized various physicochemical techniques including UV spectroscopy, FTIR spectroscopy, dynamic light scattering (DLS), transmission electron microscopy (TEM), and small-angle X-ray scattering (SAXS). Disarib-loaded P123 micelle formulation denoted as P123D exhibited a well-defined particle size of approximately 29.2 nm spherical core−shell morphology. Our investigations revealed a notable encapsulation efficiency of 75%, and we observed a biphasic release pattern for the encapsulated Disarib. Furthermore, our cytotoxicity assessment of P123D micelles against mouse breast adenocarcinoma, mouse lymphoma, and human leukemic cell lines showed 40−45% increase in cytotoxicity compared with the administration of Disarib alone in the breast adenocarcinoma cell line. Enhancement in the cytotoxicity of P123D was found to be higher or limited; however, it is important to observe that the encapsulation method significantly enhanced the aqueous solubility of Disarib as it has the best solubility in dimethyl sulfoxide (DMSO) in the unencapsulated state.
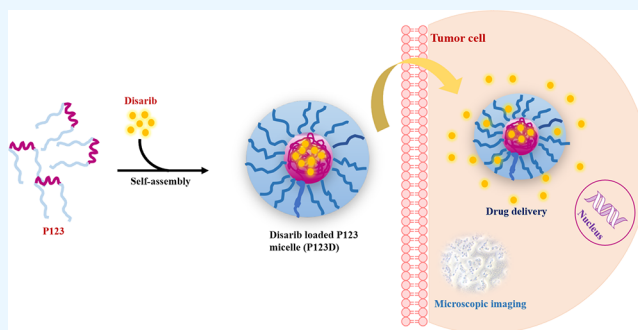
1. INTRODUCTION

Apoptosis is a highly orchestrated process that eliminates damaged and unwanted cells.[1] Cancer cells have evolved many mechanisms to evade apoptosis. The antiapoptotic protein BCL2 (B-cell lymphoma 2) is overexpressed in several types of cancer cells and contributes to prolonged cell survival and chemoresistance, lending itself as an excellent target for chemotherapeutics.[2−6] The regulation of apoptosis is critically influenced by BCL2 family proteins. They are broadly classified into two major categories: proapoptotic and antiapoptotic proteins. Over the years, several extensive investigations have been conducted on BCL2 inhibitors due to their potential as anticancer agents, as they disrupt the interaction between the heterodimer complex of antiapoptotic protein BCL2 and proapoptotic protein BAK/BAX. The prominent examples include Gossypol, AT101, Obatoclax, ABT737, ABT263, ABT199, and AT101. However, most of them were abolished before clinical use due to their severe side effects.[6−8]

Failure of ABT263 due to its nonspecificity led to the development of ABT199/ventoclax,[9,10] which showed specific binding toward BCL2 with no off-target effect. It disrupts the interaction between BCL2 and BAK or BAX, leading to homodimerization of BAK-BAK or BAX-BAX and activation of the apoptotic cascade. ABT199 is the only FDA-approved drug to treat acute myeloid leukemia and chronic lymphocytic leukemia.[11]

Disarib, a novel BCL2 inhibitor, has been shown to target tumor cells in a BCL2-specific manner, leading to a reduction in tumor burden in multiple mouse models.[5,12,13] Importantly, a head-to-head comparison of Disarib to ABT199 revealed that Disarib is more potent than ABT199.[12] Acute toxicity analysis in two rodent species revealed that even a dose as high as 2000 mg/kg of Disarib did not cause significant toxicity.[14,15] There was no significant variation in blood parameters or kidney or

liver functions following the administration of Disarib. Histological analysis of different tissues from Disarib-treated groups revealed standard architecture with no observable cellular damage.[14,15] Further, solubility tests revealed that besides dimethyl sulfoxide (DMSO), Disarib is soluble in ethanol but not in water.[15]

Nanoencapsulation of anticancer drugs represents a promising approach to setting aside the drawbacks encountered while working with traditional medicines. Nano-encapsulation has been shown to be effective in increasing the delivery efficacy with an improved solubility of potential drug candidates. Extensive investigations established that nanocarriers can act as drug delivery agents to provide a high therapeutic performance by efficient targeted drug delivery.

Pluronic block copolymers, also known as Poloxamers, are widely utilized as approved pharmaceutical additives for delivering low molecular weight drugs.[16−18] They are favored by formulators due to their easy availability in the market and their endorsement for pharmaceutical use, which enables seamless translation from basic research to medical applications. The existing literature provides several examples of successful encapsulations achieved through thin-film hydration techniques.[19−22] For instance, Pluronic P123 micelles have effectively solubilized Redaporfin, which is a photosensitizer used in cancer photodynamic therapy.[23] Moreover, xanthene dyes with varying hydrophobicity have been successfully incorporated into formulations containing P123 or F127 using thin-film method.[24] P123 is a block copolymer composed of oxyethylene (EO) units, represented as CH_2CH_2O, and oxypropylene (PO) units, represented as $CH_2CH(CH_3)O$. Hydrophobic drugs often reside in the inner hydrophobic PPO core, while the hydrophilic PEO portion acts as the outer shell. The hydrophilic PEO corona also helps to maintain the stability of the micelles.[25]

There is rapidly growing trend of nanoformulations of anticancer drugs or other less bioavailable drugs to be employed as therapeutic candidates.[26] During the past decade, the medicinal chemistry field victimized a huge transformation in drug delivery systems.[27] Stable polymeric micelles were formed using amphiphilic and reduction-responsive star copolymers that exhibit a triggered release of anticancer drug Doxorubin. Cu(I) catalyzed azide−alkyne cycloaddition was utilized for the synthesis of hyperbranched copolymers, improving the activity of self-assembled polymeric micelles.[28] Kong et al. have employed an innovative approach to create micelles that are both fluorescent and responsive to pH changes by combining fluorescent dithiomaleimide groups with pH-sensitive polymers such as poly(2-(diisopropylamino) ethyl methacrylate) and poly(2-(dibutylamino) ethyl methacrylate) through copolymerization.[29] A magnetic-responsive nanostructure based on Fe_3O_4 and poly(vinylpyrrolidone) was constructed for the controlled release of Doxorubicin, which is a versatile theranostic platform that responds to stimuli and serves multiple functions.[30]

Several studies showed many naturally occurring bioactive compounds, which are derived from natural products like berberine and resveratrol, developed into pharmaceuticals.[31−34] Nanoparticle-based formulations have been developed for the enhanced absorption and optimal delivery of the encapsulated drug to the target tissue. Such systems increase the solubility, permeation, and retention effect in the tumor sites, thereby increasing the effectivity of the formulated drug.

In this study, we report the encapsulation of Disarib using a thin-film hydration method, employing the biocompatible P123 copolymer. Our primary aim is to enhance the delivery of the novel molecule Disarib, which specifically inhibits BCL2 and exhibits higher toxicity in cancer cell lines overexpressing BCL2, through nanoencapsulation. Figure 1 shows the molecular structure of Disarib.
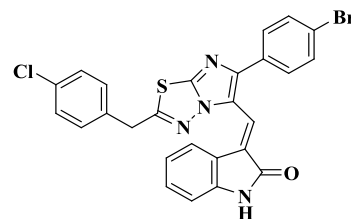

Figure 1. Disarib.

2. MATERIALS AND METHODS

Pluronic P123 and D_2O were purchased from Aldrich. All the salts and solvents used in the study were purchased from Merck, Sigma Chemical Co. (St. Louis, MO), Amresco (USA), and SRL (India). All other reagents and buffer solution components were of analytical grade preparations. Distilled and deionized water were used in all experiments.

2.1. Cell Lines and Culture. EAC (mouse breast cancer), Yac1 (T cell mouse lymphoma), and Nalm6 (B cell precursor leukemia cell line) cells were used for the cytotoxicity analysis.[13,35] Cells were cultured in RPMI 1640 or DMEM medium supplemented with 10% fetal bovine serum (FBS), 100 μg/mL penicillin, and 100 μg/mL streptomycin media and incubated at 37 °C in a humidified atmosphere containing 5% CO_2.

2.2. Preparation of Disarib-Loaded P123 Micelles (P123D). The preparation of P123D was carried out using the thin-film hydration method, as described in previous reports.[36,37] In summary, 10 mg of Disarib was mixed with 150 mg of Pluronic block copolymer P123 in 10 mL of acetonitrile. The solvent was then evaporated using a rotary evaporator at a temperature of 50 °C for approximately 1 h, resulting in the formation of solid Disarib-P123 matrix. Any remaining acetonitrile in the film was removed by vacuuming overnight at room temperature. The resulting thin film was hydrated with water and stirred at 700 rpm for 30 min to obtain a solution of micelles. This solution was subsequently filtered through a 0.2 μm filter membrane to eliminate any unincorporated drug aggregates and then subjected to lyophilization.

2.3. *In Vitro* Release Studies. For conducting release studies of Disarib from the P123 micelle, the dialysis method was adopted. The release experiments were carried out in phosphate-buffered saline (PBS) solution at pH 7.4 containing 0.2% Tween 80. Specifically, 1 mL of either free Disarib solution or P123D with pH 7.4 was placed within a dialysis bag with a molecular weight cutoff (MWCO) of 12,000 Da. Subsequently, the dialysis bag was fully immersed in 40 mL of PBS (pH 7.4) containing 0.2% Tween-80 and maintained at a temperature of 37 °C. At predefined time intervals (0, 1, 4, 8, 12, 24, 48, and 72 h), 0.5 mL aliquots were withdrawn from the medium and replaced with an equivalent volume of fresh medium. The release percentage was calculated by determining the concentration of Disarib from release media by recording

the absorbance at 385 nm by the UV−visible spectroscopy method (UV 1800, Shimadzu).

2.4. Encapsulation Efficiency. The encapsulation efficiency (EE) is determined through the utilization of eq 1.[38] The encapsulation of Disarib within the P123 micelles was evaluated using a UV−vis spectrophotometer (UV 1800, Shimadzu). Subsequently, the supernatant, obtained by centrifuging the nanoparticles at 10,000 rpm, was subjected to UV−vis spectroscopic analysis to determine the Disarib content. Absorbance was measured at 385 nm, representing the absorption maximum of Disarib. By establishing a standard calibration curve correlating the concentration with absorbance, the encapsulation efficiency was calculated using the specified equation.

$$((W - w)/W) \times 100 \tag{1}$$

where W is the amount of Disarib initially added, and w is the amount of Disarib present in the supernatant.

2.5. Fourier Transform Infrared Spectroscopy (FTIR). Potential chemical interactions between Disarib and the host P123 copolymer were studied by Fourier transform infrared spectroscopy (FTIR). The infrared (IR) spectra of free powdered Disarib and Disarib-loaded P123 micelles were measured on a Shimadzu 8400 FTIR spectrometer.

2.6. ¹H NMR Spectroscopy. NMR spectra were recorded with a JEOL JNM-ECZ400S/L1 instrument operating at 400 MHz for ^{1}H NMR in deuterated solvent (DMSO-d_6) at 295 K, unless otherwise noted. Chemical shifts (δ) are listed in parts per million (ppm) and are reported relative to solvent residual signals.

2.7. Measurement of the Particle Size and Zeta Potential. The particle size and zeta potential were determined using the dynamic light scattering (DLS) method. To perform the experiment, lyophilized P123D was dispersed in water and then subjected to sonication. The particle size analysis was conducted using a HORIBA SZ-100 nanoparticle analyzer instrument, utilizing a DPSS LASER operating at 532 nm and a scattering angle of 90°.

2.8. Small-Angle X-ray Scattering (SAXS). Small-angle X-ray scattering (SAXS) analysis was carried out using the Anton Paar SAX Space instrument.[39] A sealed tube X-ray source (Cu−Kα) with line collimation, operating at 40 kV and 50 mA and with a 2D CCD with a pixel size of 24 μm, was employed. The analysis spanned a momentum transfer range (Q) from 0.01 to 0.65 Å^{-1}. The samples were placed in a 1 mm quartz capillary and temperature-controlled using a Peltier-controlled sample holder. The distance between the sample and the detector was set to 305 mm. Quantitative information about the structure of the micelle was obtained by model-fitting the data using polydisperse core−shell sphere micelles.

2.9. Transmission Electron Microscopy (TEM). TEM images were obtained on an Igor 1200EX electron microscope, operating at 80 kV of accelerating voltage. Freshly prepared samples were prepared by dropping 5 mL aliquots of Pluronic micelle solution (H$_2$O) onto a TEM grid (400-mesh copper grid coated with carbon). After a few minutes, the remaining solution was blotted off with a filter paper, and images were collected.

2.10. Solubilization Efficiency of P123D. The solubility of Disarib alone and P123D in aqueous medium was studied.[40] A certain quantity of Disarib and P123D was suspended in water (2 mL), and vials were placed on a mechanical shaker for 24 h at room temperature. Later, the suspension was centrifuged at 6000 rpm for 15 min, and the supernatant was collected. All the samples were filtered using a 0.45 μm syringe filter and analyzed on a UV−visible spectrometer.

2.11. Stability Study of P123D. The *in vitro* stability of P123D in PBS solution was evaluated.[41] All of the samples were incubated at 4 °C for a period of 1 week. The average diameter and zeta potential of P123D were studied at different time intervals by using DLS.

2.12. Evaluation of Cytotoxicity in Cancer Cells. Cytotoxicity of P123D was assayed in various BCL2 high cancer cell lines, EAC, YAC1, and Nalm6.[12,36] A total of 25,000 cells/mL were seeded in a 24-well plate (Thermo Scientific Nunc Cell-Culture Treated multiwell plates with the Nunclon Delta surface treatment). Cells were treated with increasing concentrations of P123D. The cytotoxicity of an equivalent concentration of P123 and Disarib alone was used as a control. For P123D and Disarib alone, 0.05, 0.1, 0.2, 0.5, 1, and 2 μg/mL concentrations were used and, for polymer P123 alone, 0.74, 1.5, 3, 7.4, 14.9, and 29.7 μg/mL concentrations were used. After 48 h, the number of viable cells was ascertained by mixing cells with an equal volume of 0.4% trypan blue stain (Sigma Chemical Co., St. Louis, MO, USA).[42] The cells were counted using a hemocytometer, the cell number was plotted against a time period of cell growth using GraphPad Prism version 5, and error bars are indicated. Each experiment was repeated a minimum of three independent times (*$p < 0.05$, **$p < 0.005$, ***$p < 0.001$, and ****$p < 0.0001$).

2.13. Microscopy. To evaluate cytotoxicity caused by P123D, EAC cells were seeded and treated with P123D, Disarib alone, and P123 alone as described before after 48 h prior to trypan blue exclusion assay. For imaging, a bright-field microscope (Carl Zeiss AxioVision, Oberkochen, Germany) was used.[43−45]

2.14. Statistical Analysis. For each experiment, Student's *t* test (two-tailed), using GraphPad Prism (Version 6.01), was employed to calculate the statistical significance of the results reported. Values with a p value less than 0.05 were considered significant. Values are presented as the mean ± SEM.

3. RESULTS AND DISCUSSION

The thin film hydration technique is a commonly used method for the production of self-assembled structures, such as micelles and liposomes. This can also be employed for polymer/micelle encapsulation of various hydrophobic molecules. In this study, the encapsulation of the hydrophobic BCL2 inhibitor molecule Disarib was done within a P123 matrix using the reported technique.[36] Initially, a thin and uniform liquid crystalline film was created by dissolving Disarib and P123 in acetonitrile and evaporating the resulting film in a rotavapor. To obtain the Disarib-loaded P123 micelle (P123D), the dried film was reconstituted in an aqueous buffer. Along with the ratio of ethylene oxide (EO) units to propylene oxide (PO) units (EO/PO ratio) of Pluronic, numerous environmental factors such as the concentration, compatibility, ionic strength, and temperature affect the formation of the micellar structure. The P123D solution was lyophilized for 72 h, resulting in the formation of a powdered micellar system. Lyophilization is a significant technique in drug encapsulation because it enhances the stability of colloidal drug delivery systems by preventing leaching.[46,47]

The potential of P123 as a drug carrier has been evaluated in many studies for both *in vitro* and *in vivo* applications.
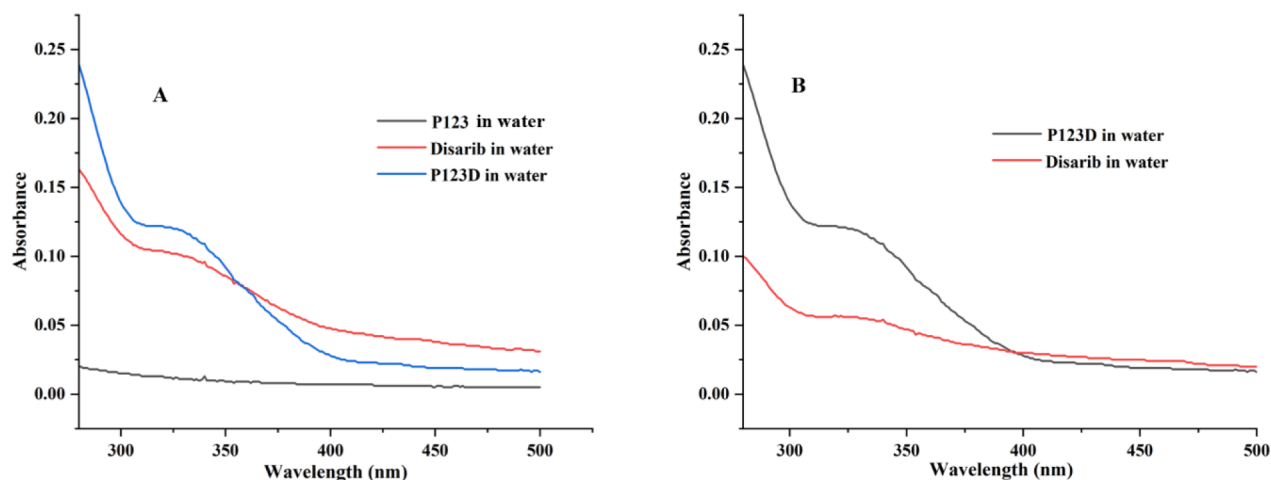
Figure 2. (A) UV−visible spectra of P123, Disarib, and P123D in water. (B) Solubility of P123D and Disarib in water.
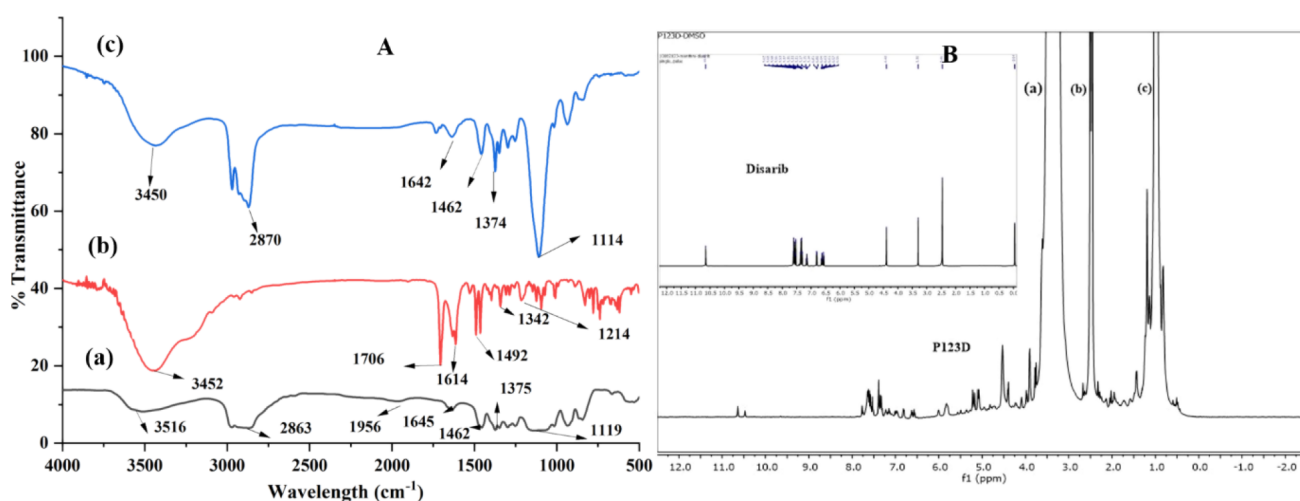

Figure 3. (A) FTIR plots of (a) P123, (b) Disarib, and (c) P123D and (B) ^{1}H NMR spectrum of P123D. Labels (a), (b), and (c) are the signals of P123 in DMSO-d_6. The ^{1}H NMR spectrum of Disarib alone in DMSO-d_6 is shown in the inset.

Similarly, in 2006, Han et al. investigated the effectiveness of Pluronic P123 loaded with paclitaxel (PTX) in terms of *in vitro* release, *in vivo* pharmacokinetics, and tissue distribution. The results indicated that P123 can effectively solubilize PTX, improve its blood circulation time and biodistribution, and protect and retain it in a biological environment.[48] Docetaxel (DTX) is an antineoplastic drug whose clinical efficacy is limited due to poor solubility, low selective distribution, etc. Liu et al. developed micelles loaded with DTX and P123, which could be administered intravenously. DTX encapsulated in P123 micelles via the thin-film hydration method enhances the bioavailability, and they investigated the release and cytotoxicity behavior. Furthermore, the *in vivo* tumor growth inhibition of the system was evaluated in Kunming mice bearing B16 tumor. The results demonstrated that the DTX-micelles have a superior *in vivo* antitumor effect than the commercially available DTX injection.[49] Later in 2013, a novel P123-DTX conjugate in which DTX is covalently conjugated to the block copolymer P123 via an ester bond was developed. The P123-DTX conjugate exhibits improved solubility of DTX and *in vivo* therapeutic efficiency.[50] Pellosi et al. reported the potential of the Pluronic mixed micelles (PMMs) as a pulmonary delivery agent for poorly water-soluble drugs. They have developed Pluronic P123/F127 mixed micelles for

the delivery of the corticosteroid budesonide (BUD), and the experiments in the mice model showed promising results. The observations confirmed that the BUD-loaded micelles were more effective than conventional BUD suspension and the inhalable PMM can be a potential platform for the delivery of lipophilic drugs to the lungs.[51]

3.1. Characterization of the Disarib-Loaded P123 Micelle System. *3.1.1. UV−Visible Spectroscopy.* The effectiveness of a drug as a therapeutic agent can be improved by enhancing its solubility in an aqueous medium. As per Raghavan et al.,[14] Disarib, the BCL2 small molecule inhibitor, has limited solubility and can only dissolve in DMSO and alcoholic systems. To determine its solubility and analyze its encapsulation in the P123 micelle, the absorption spectra were provided. Figure 2A displays the UV−visible absorption spectra of P123, Disarib, and P123D in an aqueous medium. Free P123 does not exhibit any UV absorption signal, whereas Disarib and P123D show a signal at 355 nm. The absence of a signal for P123 is due to the aliphatic saturated structure of the polymer, resulting in the negligible absorption of UV−visible light. Due to its low solubility in water, Disarib molecules only show a less intense peak in the UV−vis spectra. The intense peak obtained for P123D compared to the Disarib molecule indicates that the drug molecule shifted from the bulk phase to
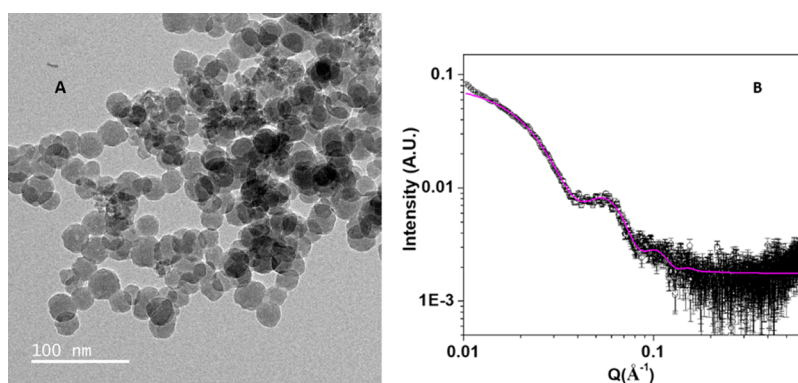
Figure 4. (A) TEM image of P123D and (B) background-subtracted SAXS pattern of P123D (magenta solid line represents the model fit).

the micellar phase, and it provides evidence for the fact that the incorporation of the hydrophobic drug was better in P123. The results were in agreement with previous reports.[52,53]

To evaluate the solubility of Disarib in aqueous medium, a certain amount of Disarib and P123D was dissolved in water, and the increase in the intensity of P123D's absorption peak in comparison to Disarib in water indicated an enhanced solubility of Disarib (Figure 2B). As per the similar works reported, Pluronic micelles are capable of solubilizing and encapsulating poorly soluble drugs due to the hydrophobic forces present in them. The interaction between the drug and Pluronic is mainly determined by the anhydrous methyl groups, even though the methyl groups contribute to both hydrophobic and hydrophilic microenvironments. The Pluronic micelle's solubilizing capacity is regulated by the number of anhydrous PO−CH3 groups, as evidenced by the high Disarib loading in the P123 micelles.[54] P123 has 69 propylene oxide units in a total mass of molecules, and it results in the high hydrophobicity of the Pluronic micelles. Furthermore, P123 has high surface activity and low CMC (critical micelle concentration), which makes it an excellent solubilizer of hydrophobic drugs.[53]

3.1.2. FTIR and NMR Studies. FTIR analysis was carried out to characterize the lyophilized nanoparticulate system and to confirm proper encapsulation of the Disarib molecule onto the P123 copolymer. The FTIR spectra of P123 copolymer, Disarib, and P123D are shown in Figure 3A. In the FTIR of the lyophilized P123D, an intense band at 1114 cm^{-1} corresponds to C−O bonds from the PEO−PPO obtained. In P123, the C−H stretching vibrations are observed in the range of 2850 to 3000 cm^{-1}, and the C−H bending vibrations appear at 1462 cm^{-1}. Peaks at 1375 cm^{-1} correspond to C−O−C stretching vibrations in P123. Additionally, the O−H stretching vibrations occur at 3516 cm^{-1} and O−H bending at 1642 cm^{-1}.[55,56] These spectral features provide valuable information about the chemical composition and structural characteristics of P123 copolymer. Disarib shows peaks at 3452, 1706, and 1614 cm^{-1} corresponding to N−H stretching, C=O stretching, and C=C stretching, respectively. When comparing the peaks of Disarib alone with those of P123D, a notable shift in signals is observed. Most of the vibrational peaks of Disarib in the range of 1500−2000 cm^{-1} are shown to be disappeared in the case of P123D. These findings strongly indicate that Disarib was effectively encapsulated within the P123 matrix, confirming the successful encapsulation process. The minimal shifts in peak positions support the stability and

compatibility of Disarib within the P123 matrix, signifying the successful integration of the drug into the micelle.

^{1}H NMR spectroscopy showed the successful encapsulation of Disarib in P123. The ^{1}H NMR spectrum of P123D, in DMSO-d_6 as the solvent, exhibited characteristic aromatic signals from Disarib at 6.5−8 ppm. The signal intensity for Disarib was much lower compared to the signal intensity for the Pluronic counterpart, as observed in Figure 3B.

3.1.3. Size and Morphological Analysis of P123D. Transmission electron microscopy (TEM) and small-angle X-ray scattering (SAXS) confirmed the spherical morphology of P123D micelles, which is shown in Figure 4A. The distribution of particle sizes plays a crucial role in the delivery of drugs. Particles smaller than 300 nm can be effectively transported through the biological system, although the P123 micelles were estimated to have a size of approximately 20 nm.[57] However, upon encapsulation of Disarib, a significant increase in the micellar size was observed. This enlargement can be attributed to the expulsion of water from the micelles and the hydrophobic nature of the Disarib-loaded particles. The expulsion of water from the system generally leads to an increase in particle size, as the hydrophobic core components tend to aggregate together, seeking to minimize their exposure to the surrounding aqueous environment.[58]

The hydrophobicity displayed by Disarib is presumed to induce strong folding of the PEO−PPO chains around the drug complexes through hydrophobic interactions. As a consequence of these interactions, water is concomitantly expelled from the core, thus contributing to the observed behavior of the size enlargement. The analysis of the Disarib-loaded P123 micelle reveals a spherical shape. From TEM images, several spherical micelle-like particles are visible, displaying a typical size in the range below 50 nm. However, a considerable number of clumps are also evident, which exhibit the presence of aggregates of some particles that formed during the solvent evaporation process.

To confirm the observations from the TEM analysis, we performed SAXS measurements to gain more insight into the system. SAXS has become a useful tool for the analysis of macromolecules, biological molecules, and nanostructures. SAXS can be used for the structural and morphological analyses of nanoparticles, particularly for particle sizes less than 100 nm. In our study, we performed the SAXS analysis of Disarib-encapsulated P123 micelles to obtain the morphology and structural dimension. Figure 4B shows the SAXS pattern of the Disarib-encapsulated P123 micelles. From the obtained SAXS pattern, it is evident that the micelles have a core−shell

Table 1. Structural Parameters of P123D Micelles As Obtained from the SAXS Analysis

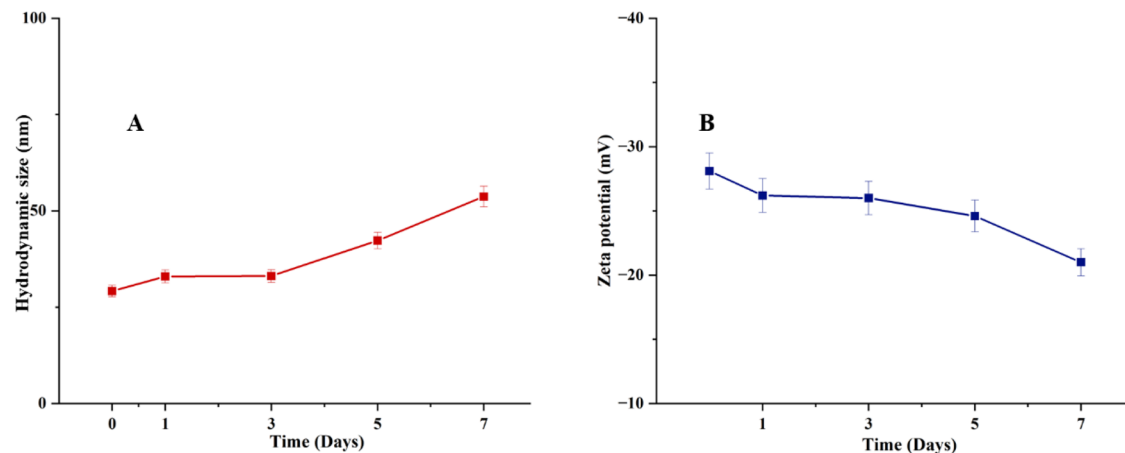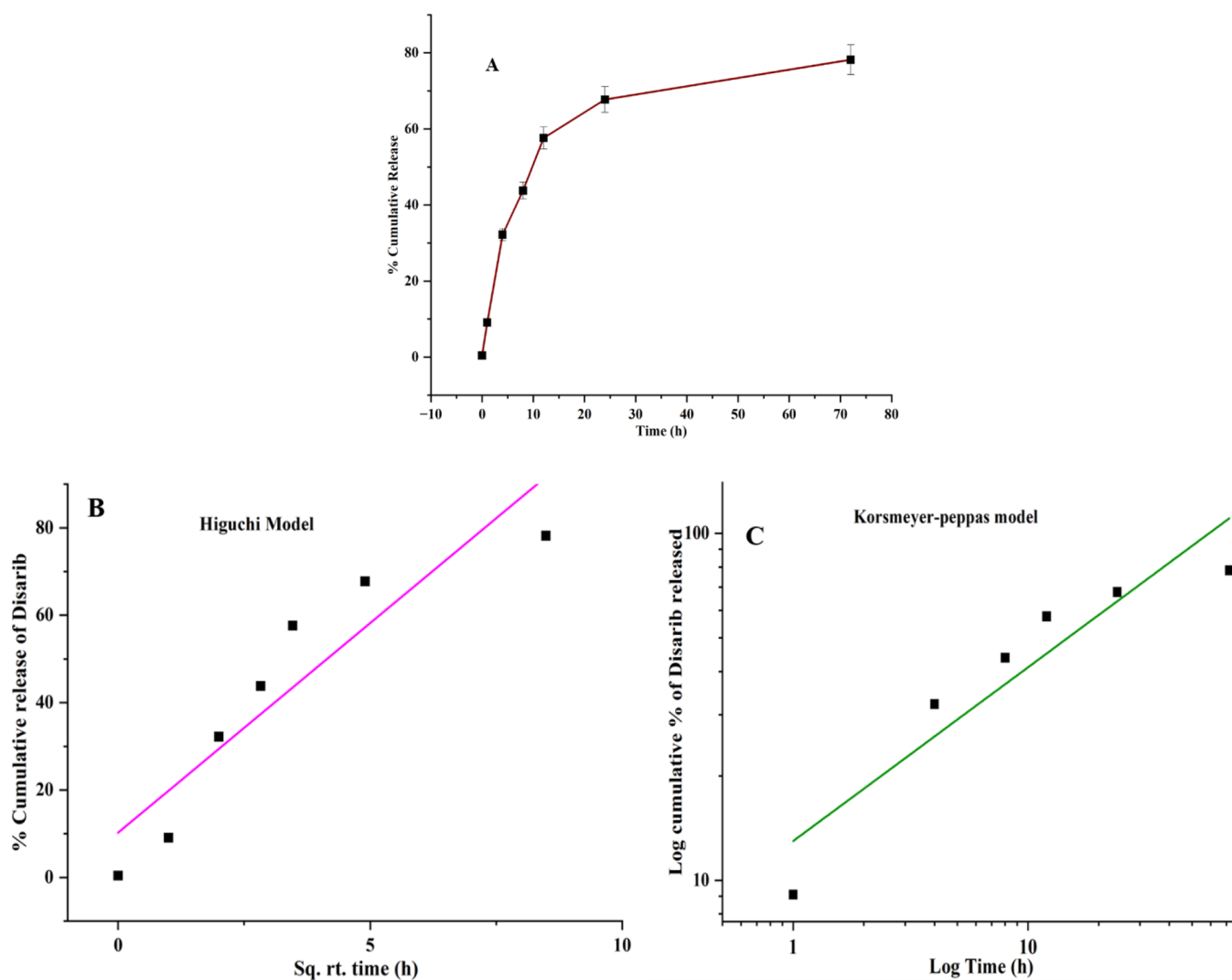| model	R_C (Å)	T_{Shell} (Å)	core SLD (10^{-6} Å^{-2})	shell SLD (10^{-6} Å^{-2})	ϕ_{HS}	χ^2
core−shell sphere	51.4 ± 0.5	32.6 ± 0.4	9.39 ± 0.1	9.87 ± 0.1	0.04 ± 0.01	1.4

Figure 5. (A) *In vitro* stability of P123D determined by hydrodynamic size measurement obtained from DLS and (B) zeta potential.

Figure 6. (A) Release profile of Disarib from P123 in 0.2% Tween 80 solution (pH 7.4), (B) Higuchi model plot of Disarib from P123D, and (C) Korsmeyer−Peppas model plot of Disarib from P123D.

spherical morphology as revealed by the shoulder peak at an intermediate scattering vector ~0.057 Å^{-1}, and the data were best fitted in the core–shell spherical model with a reduced chi-squared (χ^2) value of 1.4. A constant polydispersity of 0.1 with a Schulz distribution of sizes was applied to the core radius. The magenta-colored solid line shows the simulated scattering pattern, and the resultant radii of the core and shell thickness are 5.14 and 3.26 nm, respectively. The detailed structural parameters obtained from the model fit are listed in Table 1.

The core–shell micelle structure is highly advantageous for various applications, including drug delivery systems, as it allows hydrophobic drugs to be encapsulated within the core and shielded from the surrounding aqueous environment. This structure also offers stability and solubilization benefits for certain hydrophobic compounds in aqueous solutions.

Smaller size nanoparticles are more efficient as compared to larger-sized ones due to their enhanced efficiency in permeating biological barriers, transport through capillaries, and higher stability in the bloodstream.[59–61] From dynamic light scattering, the average particle size of P123D is found to be 29.2 nm. The zeta potential value of −28.1 mV for P123D indicates that the micelles have a relatively highly negative surface charge. This negative charge can be attributed to the presence of charged functional groups on the P123 surfactant or the encapsulated Disarib molecules. The electrostatic repulsion between negatively charged surfaces can prevent aggregation and improve the colloidal stability of micelles in solution. The prominent rise in scattering intensity observed at lower q values in the SAXS plot, compared to the model line, clearly suggests that aggregation occurs within the sample. This could plausibly account for the larger size obtained through the DLS analysis.

During a week-long evaluation of P123D, its stability at 4 °C was assessed. The particle size and zeta potential were studied, and the results are presented in Figure 5A,B, respectively. The data indicated a small increase in the hydrodynamic size of P123D micelles from 29.2 to 53.7 nm. However, the zeta potential showed no significant changes and remained within the desired range (Figure 5B). Stability is crucial for the successful delivery of hydrophobic molecules such as Disarib, as it ensures that the micelles remain dispersed and active during their journey through the body, enhancing their drug delivery efficiency.

3.2. Encapsulation Efficiency (EE). The encapsulation efficiency (EE) of the micellar formulation is significantly influenced by factors like the concentration and characteristics of Disarib, the properties of the copolymer, nature of the solvent used, and the method of encapsulation. Different drugs may show varying degrees of EE due to the difference in the characteristics of the drug, its affinity toward the copolymer, and the solvent used in the synthesis. These factors affect the overall performance of the micellar system.

The physicochemical characters of the copolymer, including its hydrophilicity/hydrophobicity and molecular weight, dictate its ability to form stable micelles. Furthermore, the choice of solvent utilized during micelle formation significantly affects the micelle formation and stability. Diverse solvents may yield different encapsulation efficiencies, influencing the overall drug loading capacity of the micellar formulation.

Last, the adopted synthetic method plays a crucial role in determining the micelle's characteristics, including size, structure, and drug-loading capabilities. Consequently, select-ing an appropriate encapsulation method is crucial to optimize the encapsulation efficiency of micellar formulations and enhance their potential as effective drug delivery systems with improved therapeutic potential. Encapsulation efficiency was determined by using UV–visible spectroscopy, where a calibration curve was created to quantify the Disarib content in the supernatant. The data revealed an encapsulation efficiency of 75% for Disarib in the P123 micelle. The Pluronic copolymer demonstrated a favorable encapsulation capacity for Disarib, which consists of aromatic and heterocyclic systems.

3.3. *In Vitro* Release Studies. The drug release kinetics of encapsulated Disarib from P123 micelles were studied at biological pH of 7.4 over a time period of 72h to mimic the bloodstream, and the release was quantified. The release profile exhibited a biphasic pattern (Figure 6A). Initially, around 32.2% of Disarib was released within the first 4 h, possibly due to surface adsorption or diffusion from the P123 matrix. The initial burst release of the drug facilitated the rapid achievement of therapeutically effective drug concentrations in the bloodstream. Subsequently, a sustained release phase ensued, with approximately 78.2% of Disarib released over 72h. During this phase, Disarib was gradually released from the micellar matrix. This sustained release mechanism may be advantageous, as it can help to maintain consistent and effective drug concentration in the bloodstream. In accordance with previous reports, the quick release is occurring since micelles exhibit dynamic equilibrium with the bulk solvent and at extensive dilution equilibrium shifts toward dissociation. This explains the initial quick release of Disarib.[54]

3.4. Drug Delivery and Kinetics. The cumulative drug release data were analyzed using various kinetic release models such as Higuchi and Korsmeyer−Peppas to elucidate the mechanism of drug release. Initially, the data were fitted into the Higuchi square root model, which involves plotting the % cumulative release against the square root of time (Figure 6B). The equation is

$$Q = k \times t^{0.5} \tag{2}$$

In the Higuchi square root model, where Q represents the cumulative amount of drug released at time t and k is the Higuchi dissolution constant. A linear relationship was observed with a high regression value of 0.823. This indicates that drug release occurs via a diffusion mechanism.

Apart from the Higuchi model, the data were fitted into the Korsmeyer−Peppas model (Figure 6C). In this case, the data were plotted as log cumulative release versus log time in hours. The equation is

$$Q = k_2 \times t^n \tag{3}$$

In this context, Q represents the cumulative amount of drug released at time t, k_2 denotes the rate constant, and n signifies the diffusional exponent. We obtained the value of n, which is 0.5, confirming the diffusion mechanism as Fickian diffusion.

When the release exponent (n) in the Korsmeyer−Peppas model is 0.5, this indicates that the drug release mechanism from P123D follows Fickian diffusion, which is also referred to as Case I transport.

In the Korsmeyer−Peppas model:

$$Q = k_2 \times t^n$$
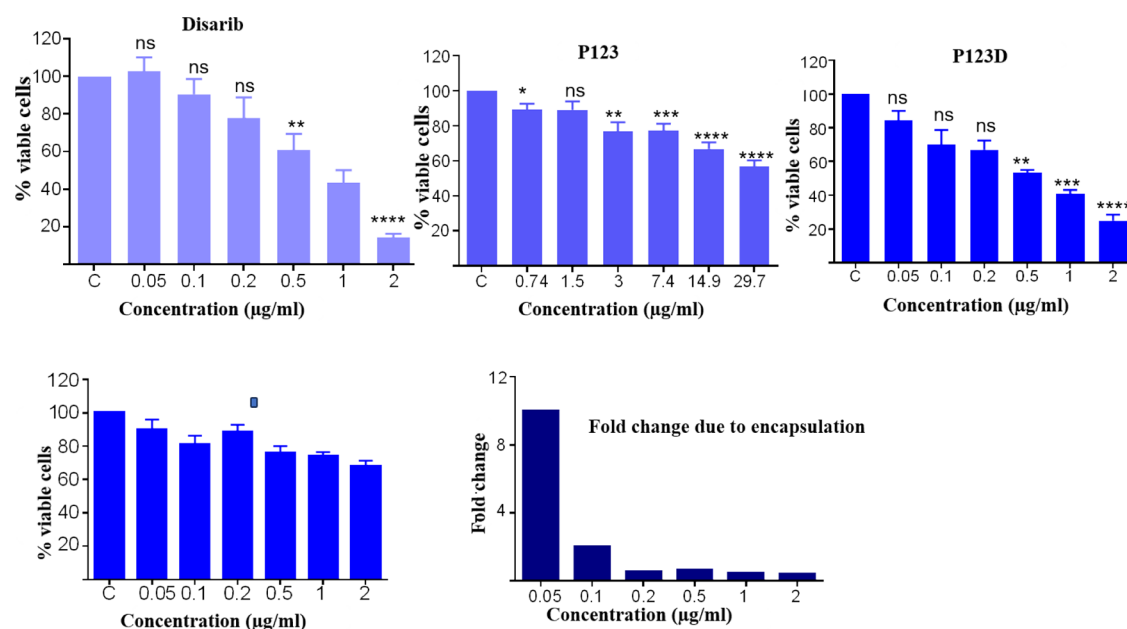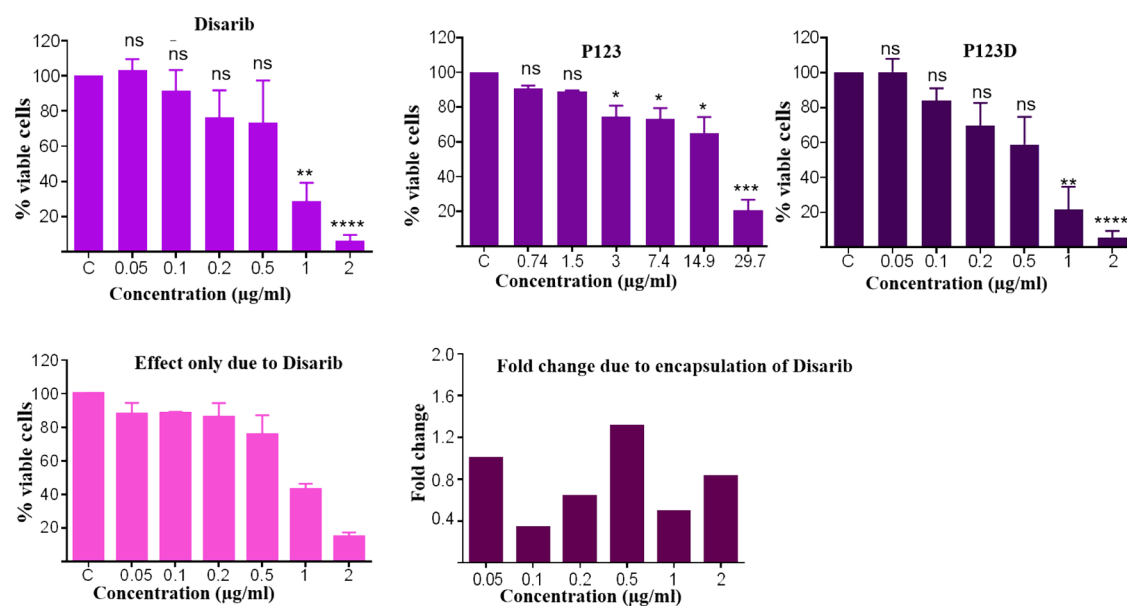
When n = 0.5, the equation becomes

Figure 7. Evaluation of the cytotoxicity of P123D in Nalm6 cell lines. Evaluation of cytotoxicity following 48 h treatment with Disarib, P123, and P123D in Nalm6. Concentrations of 0, 0.05, 0.1, 0.2, 0.5, 1, and 2 μg/mL of P123D and Disarib alone were used, whereas equivalent concentrations of 0, 0.74, 1.5, 3, 7.4, 14.9, and 29.7 μg/mL of P123 were used. Each experiment was performed a minimum of three times, and the graph shows the mean + SEM. Each experiment was repeated a minimum of three independent times ($*p < 0.05$, $**p < 0.005$, $***p < 0.001$, and $****p < 0.0001$).

Figure 8. Evaluation of the cytotoxicity of P123D in Yac1 cell lines. Evaluation of cytotoxicity following 48 h treatment with Disarib, P123, and P123D in Yac1. Concentrations of 0, 0.05, 0.1, 0.2, 0.5, 1, and 2 μg/mL of P123D and Disarib alone were used, whereas equivalent concentrations of 0, 0.74, 1.5, 3, 7.4, 14.9, and 29.7 μg/mL of P123 were used. Each experiment was performed a minimum of three times, and the graph shows the mean + SEM. Each experiment was repeated a minimum of three independent times ($*p < 0.05$, $**p < 0.005$, $***p < 0.001$, and $****p < 0.0001$).

$$Q = k \times t^{0.5}$$

This equation illustrates that the cumulative amount of drug released (Q) is directly proportional to the square root of the time ($t^{0.5}$). The square root time dependency suggests that the drug release primarily occurs through diffusion within the matrix of the dosage form. Fickian diffusion is a common mechanism observed in many drug delivery systems, especially in matrix-type systems, where the drug is dispersed throughout the matrix and subsequently releases as it diffuses through the

matrix material. It is essential to recognize that when the value of n is precisely 0.5 in the Korsmeyer–Peppas model, it represents an ideal Fickian release behavior. However, in practical applications, slight deviations from this ideal behavior may occur due to various factors, such as excipient interactions and solubility effects.

3.5. *In Vitro* Cytotoxicity Studies. trypan blue exclusion assay was performed to determine the viability in two different BCL2 high cancer cell lines (Nalm6 and Yac1) following treatment with an encapsulated version of Disarib, P123D. An
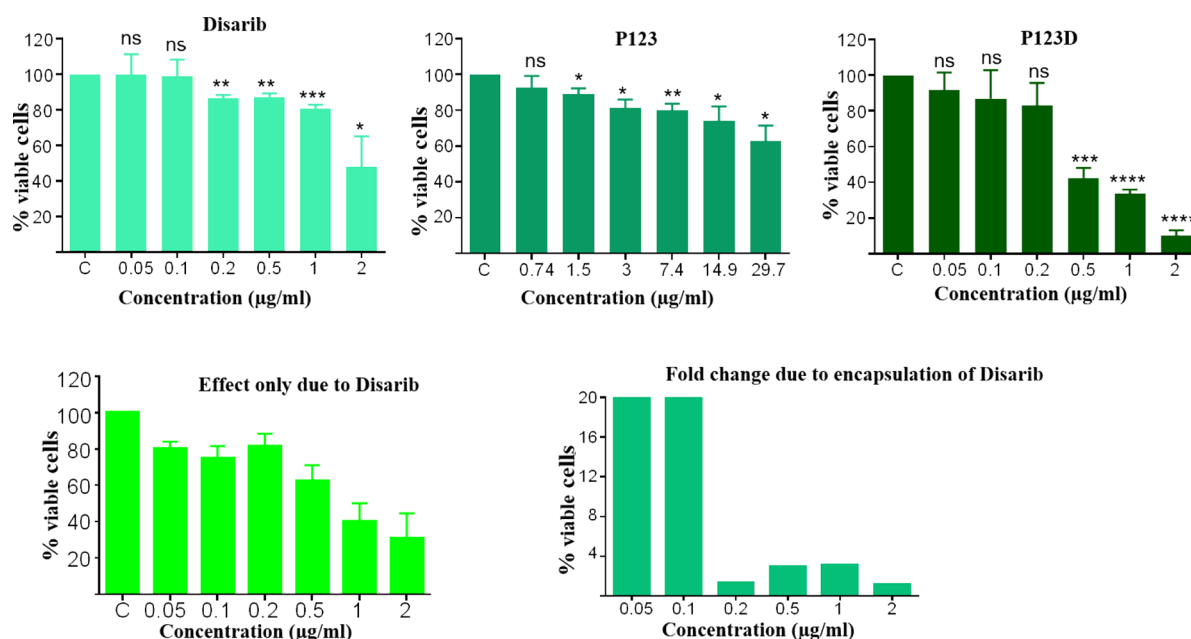
Figure 9. Evaluation of the cytotoxicity of encapsulated Disarib in the breast adenocarcinoma (EAC) cancer cell line: 0, 0.05, 0.1, 0.2, 0.5, 1, and 2 μg/mL concentrations of P123D and Disarib alone were used, whereas equivalent concentrations of 0, 0.74, 1.5, 3, 7.4, 14.9, and 29.7 μg/mL of P123 were used. Each experiment was performed a minimum of three times, and the graph shows the mean + SEM. Each experiment was repeated a minimum of three independent times (*$p < 0.05$, **$p < 0.005$, ***$p < 0.001$, and ****$p < 0.0001$).
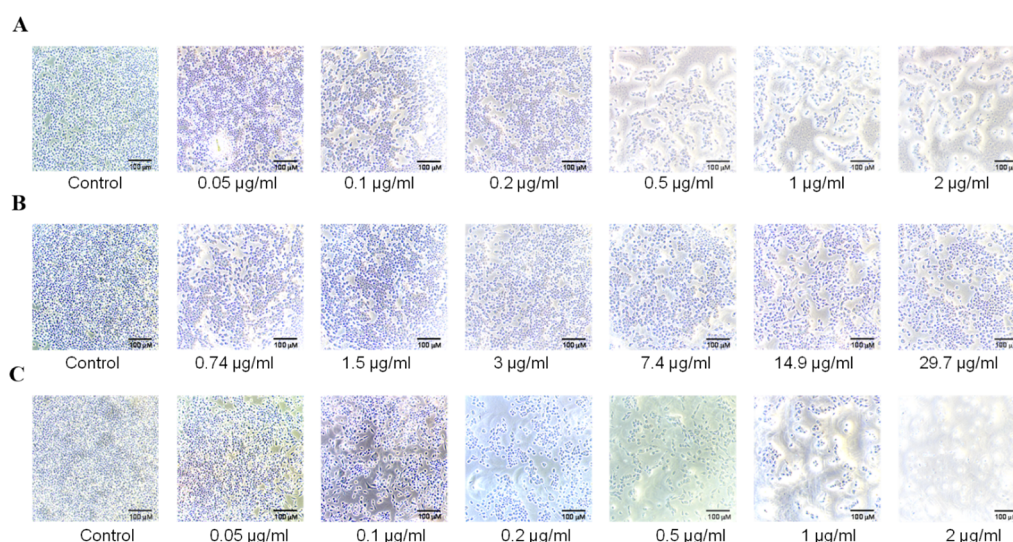

Figure 10. Evaluation of cell proliferation of breast adenocarcinoma cancer cells post 48 h treatment of encapsulated Disarib. After 48 h of treatment with Disarib alone, P123, and P123D, images of cells were captured from each concentration using a bright-field microscope. Images shown are with a magnification of 10×. (A) Representative image depicting the control and 0.05, 0.1, 0.2, 0.5, 1, and 2 μg/mL Disarib alone. (B) Representative image depicting the control and 0.74, 1.5, 3, 7.4, 14.9, and 29.7 μg/mL P123. (C) Representative image depicting the control and 0.05, 0.1, 0.2, 0.5, 1, and 2 μg/mL P123D. Scale bar, 100 μm.

equivalent concentration of P123 was used as a control to evaluate the effect of Disarib alone in encapsulated form. Our results reveal that Disarib alone and P123D showed similar efficiency in terms of cytotoxic effect in the Nalm6 cell line, and no increase in cytotoxicity was observed when treated with P123D compared to the purified form alone (Figure 7 and Figure 8). Although the impact on improving the cytotoxicity was minimal, it is important to note that encapsulation improved the solubility of Disarib in water as the unencapsulated form of Disarib was soluble only in DMSO.

To evaluate the cytotoxicity of P123D, in the breast adenocarcinoma cell line, the EAC cells were treated with the encapsulated version. While P123 alone was used as the negative control, cells treated with Disarib alone (dissolved in DMSO) served as the positive control. After 48 h of treatment, a 40−45% increase in the cytotoxicity was observed compared to Disarib alone (Figure 9). Thus, our results reveal that when encapsulated Disarib was used for the treatment of EAC cells, improved efficacy as well as solubility in water was observed. In addition, microscopic evaluation of cells after treatment with

P123D confirmed the improved cell death induced by P123D compared to Disarib alone (Figure 10).

Therefore, this work focuses on introducing an encapsulated version of a novel BCL2 inhibitor, Disarib, which specifically works against the BH1 domain of the antiapoptotic protein BCL2 to improve its efficacy and solubility *in vivo*.

4. CONCLUSIONS

A nanosystem based on Pluronic P123 has been successfully developed for the efficient delivery of the BCL2 small molecule inhibitor Disarib. The solubility and stability of Disarib were significantly improved by creating a nanomicelle formulation using a thin-film hydration technique. The resulting nanoparticle size was 29.2 nm with a spherical core–shell morphology and demonstrated a high encapsulation efficiency of 75%.

In vitro release studies showed a biphasic release pattern with an initial burst release followed by sustained and controlled release of Disarib. Moreover, cytotoxicity assays indicated that the nanoparticles effectively inhibited the growth of the breast adenocarcinoma cell line EAC, leading to cell death. Microscopic imaging confirmed that the Disarib-loaded P123 (P123D) system showed 40−45% enhancement in cell death as compared to free Disarib.

This study highlights the promising delivery and controlled release of Disarib, a novel BCL2 inhibitor, which specifically works against the BH1 domain of the antiapoptotic protein BCL2, thereby improving its efficacy and solubility *in vivo*.

■ AUTHOR INFORMATION

Corresponding Author

Jinu George − *Bio-organic Laboratory, Department of Chemistry, Sacred Heart College, Kochi 682013, India;* orcid.org/0000-0002-8802-6760; Email: jinujacob@shcollege.ac.in

Authors

Reshma Joy − *Bio-organic Laboratory, Department of Chemistry, Sacred Heart College, Kochi 682013, India*

Humaira Siddiqua − *Department of Biochemistry, Indian Institute of Science, Bangalore 560012, India*

Shivangi Sharma − *Department of Biochemistry, Indian Institute of Science, Bangalore 560012, India*

Manthra Raveendran − *Department of Biochemistry, Indian Institute of Science, Bangalore 560012, India*

Franklin John − *Bio-organic Laboratory, Department of Chemistry, Sacred Heart College, Kochi 682013, India;* orcid.org/0000-0002-3340-0858

Puthusserickal Abdulrahiman Hassan − *Chemistry Division, Bhabha Atomic Research Centre, Mumbai 400085, India*

Santosh L Gawali − *Chemistry Division, Bhabha Atomic Research Centre, Mumbai 400085, India*

Sathees C. Raghavan − *Department of Biochemistry, Indian Institute of Science, Bangalore 560012, India*

Complete contact information is available at:
https://pubs.acs.org/10.1021/acsomega.3c05802

■ REFERENCES

(1) Reed, J. C. Apoptosis-Targeted Therapies for Cancer. *Cancer Cell* **2003**, *3* (1), 17−22.

(2) Anagnostou, V. K.; Lowery, F. J.; Zolota, V.; Tzelepi, V.; Gopinath, A.; Liceaga, C.; Panagopoulos, N.; Frangia, K.; Tanoue, L.; Boffa, D.; Gettinger, S.; Detterbeck, F.; Homer, R. J.; Dougenis, D.; Rimm, D. L.; Syrigos, K. N. High Expression of BCL-2 Predicts Favorable Outcome in Non-Small Cell Lung Cancer Patients with Non Squamous Histology. *BMC Cancer* **2010**, *10*, 1−11.

(3) Catz, S. D.; Johnson, J. L. BCL-2 in Prostate Cancer: A Minireview. *Apoptosis* **2003**, *8*, 29−37.

(4) Hague, A.; Moorghen, M.; Hicks, D.; Chapman, M.; Paraskeva, C. BCL-2 Expression in Human Colorectal Adenomas and Carcinomas. *Oncogene* **1994**, *9* (11), 3367−3370.

(5) Iyer, D.; Vartak, S. V.; Mishra, A.; Goldsmith, G.; Kumar, S.; Srivastava, M.; Hegde, M.; Gopalakrishnan, V.; Glenn, M.; Velusamy, M.; Choudhary, B.; Kalakonda, N.; Karki, S. S.; Surolia, A.; Raghavan, S. C. Identification of a Novel BCL 2-Specific Inhibitor That Binds Predominantly to the BH 1 Domain. *FEBS J.* **2016**, *283* (18), 3408−3437.

(6) Radha, G.; Raghavan, S. C. BCL2: A Promising Cancer Therapeutic Target. *Biochim. Biophys. Acta BBA-Rev. Cancer* **2017**, *1868* (1), 309−314.

(7) Zerp, S. F.; Stoter, R.; Kuipers, G.; Yang, D.; Lippman, M. E.; van Blitterswijk, W. J.; Bartelink, H.; Rooswinkel, R.; Lafleur, V.; Verheij, M. AT-101, a Small Molecule Inhibitor of Anti-Apoptotic Bcl-2 Family Members, Activates the SAPK/JNK Pathway and Enhances Radiation-Induced Apoptosis. *Radiat. Oncol.* **2009**, *4*, 1−10.

(8) Zhai, D.; Jin, C.; Satterthwait, A. C.; Reed, J. C. Comparison of Chemical Inhibitors of Antiapoptotic Bcl-2-Family Proteins. *Cell Death Differ.* **2006**, *13* (8), 1419−1421.

(9) Cang, S.; Iragavarapu, C.; Savooji, J.; Song, Y.; Liu, D. ABT-199 (Venetoclax) and BCL-2 Inhibitors in Clinical Development. *J. Hematol. Oncol.* **2015**, *8* (1), 1−8.

(10) Mullard, A. Pioneering Apoptosis-Targeted Cancer Drug Poised for FDA Approval: AbbVie's BCL-2 Inhibitor Venetoclax—the Leading Small-Molecule Protein-Protein Interaction Inhibitor—Could Soon Become the First Marketed Drug to Directly Target the Ability of Cancer Cells to Evade Apoptosis. *Nat. Rev. Drug Discovery* **2016**, *15* (3), 147−150.

(11) Souers, A. J.; Leverson, J. D.; Boghaert, E. R.; Ackler, S. L.; Catron, N. D.; Chen, J.; Dayton, B. D.; Ding, H.; Enschede, S. H.;

Fairbrother, W. J.; Huang, D. C. S.; Hymowitz, S. G.; Jin, S.; Khaw, S. L.; Kovar, P. J.; Lam, L. T.; Lee, J.; Maecker, H. L.; Marsh, K. C.; Mason, K. D.; Mitten, M. J.; Nimmer, P. M.; Oleksijew, A.; Park, C. H.; Park, C. M.; Phillips, D. C.; Roberts, A. W.; Sampath, D.; Seymour, J. F.; Smith, M. L.; Sullivan, G. M.; Tahir, S. K.; Tse, C.; Wendt, M. D.; Xiao, Y.; Xue, J. C.; Zhang, H.; Humerickhouse, R. A.; Rosenberg, S. H.; Elmore, S. W. ABT-199, a Potent and Selective BCL-2 Inhibitor, Achieves Antitumor Activity While Sparing Platelets. *Nat. Med.* **2013**, *19* (2), 202−208.

(12) Vartak, S. V.; Hegde, M.; Iyer, D.; Gaikwad, S.; Gopalakrishnan, V.; Srivastava, M.; Karki, S. S.; Choudhary, B.; Ray, P.; Santhoshkumar, T. R.; Raghavan, S. C. A Novel Inhibitor of BCL2, Disarib Abrogates Tumor Growth While Sparing Platelets, by Activating Intrinsic Pathway of Apoptosis. *Biochem. Pharmacol.* **2016**, *122*, 10−22.

(13) Vartak, S. V.; Iyer, D.; Santhoshkumar, T. R.; Sharma, S.; Mishra, A.; Goldsmith, G.; Srivastava, M.; Srivastava, S.; Karki, S. S.; Surolia, A.; Choudhary, B.; Raghavan, S. C. Novel BCL2 Inhibitor, Disarib Induces Apoptosis by Disruption of BCL2-BAK Interaction. *Biochem. Pharmacol.* **2017**, *131*, 16−28.

(14) Sharma, S.; Varsha, K. K.; Kumari, S.; Gopalakrishnan, V.; Jose, A. E.; Choudhary, B.; Mantelingu, K.; Raghavan, S. C. Acute Toxicity Analysis of Disarib, an Inhibitor of BCL2. *Sci. Rep.* **2020**, *10* (1), 15188.

(15) Sharma, S.; Varsha, K. K.; Ray, U.; Siddiqua, H.; Jose, A. E.; Muninarasimaiah, S.; Raghavan, S. C.; Choudhary, B. Acute Toxicity Analysis of an Inhibitor of BCL2, Disarib, in Rats. *Sci. Rep.* **2021**, *11* (1), 9982.

(16) Pourjavadi, A.; Asgari, S.; Hosseini, S. H.; Akhlaghi, M. Codelivery of Hydrophobic and Hydrophilic Drugs by Graphene-Decorated Magnetic Dendrimers. *Langmuir* **2018**, *34* (50), 15304−15318.

(17) Pellosi, D. S.; Calori, I. R.; de Paula, L. B.; Hioka, N.; Quaglia, F.; Tedesco, A. C. Multifunctional theranostic Pluronic Mixed Micelles Improve Targeted Photoactivity of Verteporfin in Cancer Cells. *Mater. Sci. Eng., C* **2017**, *71*, 1−9.

(18) Ai, X.; Zhong, L.; Niu, H.; He, Z. Thin-Film Hydration Preparation Method and Stability Test of DOX-Loaded Disulfide-Linked Polyethylene Glycol 5000-Lysine-Di-Tocopherol Succinate Nanomicelles. *Asian J. Pharm. Sci.* **2014**, *9* (5), 244−250.

(19) Bhattacharjee, J.; Verma, G.; Aswal, V. K.; Patravale, V.; Hassan, P. A. Microstructure, Drug Binding and Cytotoxicity of Pluronic P123−Aerosol OT Mixed Micelles. *RSC Adv.* **2013**, *3* (45), 23080−23089.

(20) Ganguly, R.; Kunwar, A.; Dutta, B.; Kumar, S.; Barick, K. C.; Ballal, A.; Aswal, V. K.; Hassan, P. A. Heat-Induced Solubilization of Curcumin in Kinetically Stable Pluronic P123 Micelles and Vesicles: An Exploit of Slow Dynamics of the Micellar Restructuring Processes in the Aqueous Pluronic System. *Colloids Surf. B Biointerfaces* **2017**, *152*, 176−182.

(21) Zhao, L.-Y.; Zhang, W.-M. Recent Progress in Drug Delivery of Pluronic P123: Pharmaceutical Perspectives. *J. Drug Target.* **2017**, *25* (6), 471−484.

(22) Luo, H.; Jiang, K.; Liang, X.; Hua, C.; Li, Y.; Liu, H. Insights into Morphological Transition of Pluronic P123 Micelles as a Function of Gallate. *Colloids Surf. Physicochem. Eng. Asp.* **2019**, *572*, 221−229.

(23) Pucelik, B.; Arnaut, L. G.; Stochel, G.; Dabrowski, J. M. Design of Pluronic-Based Formulation for Enhanced Redaporfin-Photo-dynamic Therapy against Pigmented Melanoma. *ACS Appl. Mater. Interfaces* **2016**, *8* (34), 22039−22055.

(24) Managa, M.; Ngoy, B. P.; Nyokong, T. The Photophysical Studies of Pluronic F127/P123 Micelle Mixture System Loaded with Metal Free and Zn 5, 10, 15, 20-Tetrakis [4-(Benzyloxy) Phenyl] Porphyrins. *J. Photochem. Photobiol. Chem.* **2017**, *339*, 49−58.

(25) Löf, D.; Tomsic, M.; Glatter, O.; Fritz-Popovski, G.; Schillén, K. Structural Characterization of Nonionic Mixed Micelles Formed by C12EO6 Surfactant and P123 Triblock Copolymer. *J. Phys. Chem. B* **2009**, *113* (16), 5478−5486.

(26) Wang, Z.; Li, R.; Zhang, J. On-Demand Drug Delivery of Triptolide and Celastrol by Poly(Lactic-Co-Glycolic Acid) Nano-particle/Triglycerol Monostearate-18 Hydrogel Composite for Rheumatoid Arthritis Treatment. *Adv. Compos. Hybrid Mater.* **2022**, *5* (4), 2921−2935.

(27) Joy, R.; George, J.; John, F. Brief Outlook on Polymeric Nanoparticles, Micelles, Niosomes, Hydrogels and Liposomes: Preparative Methods and Action. *ChemistrySelect* **2022**, *7* (6), No. e202104045.

(28) Zhang, S.; Hou, Y.; Chen, H.; Liao, Z.; Chen, J.; Xu, B. B.; Kong, J. Reduction-Responsive Amphiphilic Star Copolymers with Long-Chain hyperbranched Poly (ε-Caprolactone) Core and Disulfide Bonds for Trigger Release of Anticancer Drugs. *Eur. Polym. J.* **2018**, *108*, 364−372.

(29) Bai, T.; Shao, D.; Chen, J.; Li, Y.; Xu, B. B.; Kong, J. pH-Responsive Dithiomaleimide-Amphiphilic Block Copolymer for Drug Delivery and Cellular Imaging. *J. Colloid Interface Sci.* **2019**, *552*, 439−447.

(30) Wang, X.; Qi, Y.; Hu, Z.; Jiang, L.; Pan, F.; Xiang, Z.; Xiong, Z.; Jia, W.; Hu, J.; Lu, W. Fe3O4@PVP@DOX Magnetic Vortex Hybrid nanostructures with Magnetic-Responsive Heating and Controlled Drug Delivery Functions for Precise Medicine of Cancers. *Adv. Compos. Hybrid Mater.* **2022**, *5* (3), 1786−1798.

(31) Habtemariam, S. Recent Advances in berberine Inspired Anticancer Approaches: From Drug Combination to Novel Formulation Technology and Derivatization. *Molecules* **2020**, *25* (6), 1426.

(32) Javed Iqbal, M.; Quispe, C.; Javed, Z.; Sadia, H.; Qadri, Q. R.; Raza, S.; Salehi, B.; Cruz-Martins, N.; Abdulwanis Mohamed, Z.; Sani Jaafaru, M.; Abdull Razis, A. F.; Sharifi-Rad, J. Nanotechnology-Based Strategies for berberine Delivery System in Cancer Treatment: Pulling Strings to Keep berberine in Power. *Front. Mol. Biosci.* **2021**, *7*, No. 624494.

(33) Annaji, M.; Poudel, I.; Boddu, S. H. S.; Arnold, R. D.; Tiwari, A. K.; Babu, R. J. Resveratrol-Loaded Nanomedicines for Cancer Applications. *Cancer Rep.* **2021**, *4* (3), No. e1353.

(34) Qin, L.; Jing, G.; Cui, N.; Xu, Z.; He, Y.; Qin, Y.; Lu, T.; Sun, J.; Du, A.; Wang, S. Resveratrol-Silica Aerogel Nanodrug Complex System Enhances the Treatment of Sports Osteoarthritis by Activating SIRT-1. *Adv. Compos. Hybrid Mater.* **2023**, *6* (1), 3.

(35) Srivastava, M.; Nambiar, M.; Sharma, S.; Karki, S. S.; Goldsmith, G.; Hegde, M.; Kumar, S.; Pandey, M.; Singh, R. K.; Ray, P.; Natarajan, R.; Kelkar, M.; De, A.; Choudhary, B.; Raghavan, S. C. An Inhibitor of Nonhomologous End-Joining Abrogates Double-Strand Break Repair and Impedes Cancer Progression. *Cell* **2012**, *151* (7), 1474−1487.

(36) John, F.; George, J.; Vartak, S. V.; Srivastava, M.; Hassan, P. A.; Aswal, V. K.; Karki, S. S.; Raghavan, S. C. Enhanced Efficacy of Pluronic Copolymer Micelle Encapsulated SCR7 against Cancer Cell Proliferation. *Macromol. Biosci.* **2015**, *15* (4), 521−534.

(37) Fares, A. R.; ElMeshad, A. N.; Kassem, M. A. Enhancement of Dissolution and Oral Bioavailability of Lacidipine via Pluronic P123/F127 Mixed Polymeric Micelles: Formulation, Optimization Using Central Composite Design and in Vivo Bioavailability Study. *Drug Delivery* **2018**, *25* (1), 132−142.

(38) Ghosh, P.; Bag, S.; Singha Roy, A.; Subramani, E.; Chaudhury, K.; Dasgupta, S. Solubility Enhancement of Morin and Epicatechin through Encapsulation in an Albumin Based nanoparticulate System and Their Anticancer Activity against the MDA-MB-468 Breast Cancer Cell Line. *RSC Adv.* **2016**, *6* (103), 101415−101429.

(39) Patel, D.; Gawali, S. L.; Kuperkar, K.; Hassan, P. A.; Bahadur, P. Co-Micellization Conduct and Structural Dynamics of Block Copolymers in Water and Salt Solution Environment for Drug Solubilization Enhancement. *Colloid Polym. Sci.* **2023**, *919*−13.

(40) Zhao, L.; Shi, Y.; Zou, S.; Sun, M.; Li, L.; Zhai, G. Formulation and in Vitro Evaluation of Quercetin Loaded Polymeric Micelles Composed of Pluronic P123 and Da-Tocopheryl Polyethylene Glycol Succinate. *J. Biomed. Nanotechnol.* **2011**, *7* (3), 358−365.

(41) Dhakar, N. K.; Caldera, F.; Bessone, F.; Cecone, C.; Pedrazzo, A. R.; Cavalli, R.; Dianzani, C.; Trotta, F. Evaluation of Solubility Enhancement, Antioxidant Activity, and Cytotoxicity Studies of Kynurenic Acid Loaded Cyclodextrin Nanosponge. *Carbohydr. Polym.* **2019**, *224*, No. 115168.

(42) Srivastava, S.; Somasagara, R. R.; Hegde, M.; Nishana, M.; Tadi, S. K.; Srivastava, M.; Choudhary, B.; Raghavan, S. C. Quercetin, a Natural Flavonoid Interacts with DNA, Arrests Cell Cycle and Causes Tumor Regression by Activating Mitochondrial Pathway of Apoptosis. *Sci. Rep.* **2016**, *6* (1), 1−13.

(43) Dahal, S.; Siddiqua, H.; Sharma, S.; Babu, R. K.; Rathore, D.; Sharma, S.; Raghavan, S. C. Unleashing a Novel Function of Endonuclease G in Mitochondrial Genome Instability. *eLife* **2022**, *11*, No. e69916.

(44) Kumari, N.; Vartak, S. V.; Dahal, S.; Kumari, S.; Desai, S. S.; Gopalakrishnan, V.; Choudhary, B.; Raghavan, S. C. G-Quadruplex Structures Contribute to Differential Radiosensitivity of the Human Genome. *Iscience* **2019**, *21*, 288−307.

(45) Sebastian, R.; Raghavan, S. C. Exposure to Endosulfan Can Result in Male Infertility Due to Testicular Atrophy and Reduced Sperm Count. *Cell Death Discovery* **2015**, *1* (1), 1−10.

(46) Kadam, Y.; Yerramilli, U.; Bahadur, A.; Bahadur, P. Micelles from PEO−PPO−PEO Block Copolymers as Nanocontainers for Solubilization of a Poorly Water Soluble Drug Hydrochlorothiazide. *Colloids Surf. B Biointerfaces* **2011**, *83* (1), 49−57.

(47) Pellosi, D. S.; Tessaro, A. L.; Moret, F.; Gaio, E.; Reddi, E.; Caetano, W.; Quaglia, F.; Hioka, N. Pluronic® Mixed Micelles as Efficient Nanocarriers for Benzoporphyrin Derivatives Applied to Photodynamic Therapy in Cancer Cells. *J. Photochem. Photobiol. Chem.* **2016**, *314*, 143−154.

(48) Han, L.; Guo, J.; Zhang, L.; Wang, Q.; Fang, X. Pharmacokinetics and Biodistribution of Polymeric Micelles of Paclitaxel with Pluronic P123. *Acta Pharmacol. Sin.* **2006**, *27* (6), 747−753.

(49) Liu, Z.; Liu, D.; Wang, L.; Zhang, J.; Zhang, N. Docetaxel-Loaded Pluronic P123 Polymeric Micelles: In Vitro and in Vivo Evaluation. *Int. J. Mol. Sci.* **2011**, *12* (3), 1684−1696.

(50) Liu, Z.; Wang, Y.; Zhang, J.; Li, M.; Liu, Y.; Zhang, N. Pluronic P123-Docetaxel Conjugate Micelles: Synthesis, Characterization, and Antitumor Activity. *J. Biomed. Nanotechnol.* **2013**, *9* (12), 2007−2016.

(51) Pellosi, D. S.; d'Angelo, I.; Maiolino, S.; Mitidieri, E.; d'Emmanuele di Villa Bianca, R.; Sorrentino, R.; Quaglia, F.; Ungaro, F. In Vitro/in Vivo Investigation on the Potential of Pluronic® Mixed Micelles for Pulmonary Drug Delivery. *Eur. J. Pharm. Biopharm.* **2018**, *130*, 30−38.

(52) John, F.; George, J.; Srivastava, M.; Hassan, P. A.; Aswal, V. K.; Karki, S. S.; Raghavan, S. C. Pluronic Copolymer Encapsulated SCR7 as a Potential Anticancer Agent. *Faraday Discuss.* **2015**, *177*, 155−161.

(53) Shaikh, S. J.; Patel, H. S.; Ray, D.; Aswal, V. K.; Singh, S.; Vijayvargia, R.; Sheth, U.; Sharma, R. K. Enhanced Solubility and Oral Bioavailability of Hydrophobic Drugs Using Pluronic Nanomicelles: An In-Vitro Evaluation. *ChemistrySelect* **2021**, *6* (28), 7040−7048.

(54) Tiwari, S.; Ma, J.; Rathod, S.; Bahadur, P. Solubilization of Quercetin in P123 Micelles: Scattering and NMR Studies. *Colloids Surf. Physicochem. Eng. Asp.* **2021**, *621*, 126555.

(55) Koganti, V. R.; Das, S.; Rankin, S. E. In Situ FTIR Investigation of the Kinetics of Silica Polycondensation in Surfactant Templated, Mesostructured Thin Films. *J. Phys. Chem. C* **2014**, *118* (33), 19450−19461.

(56) Cao, S.-W.; Zhu, Y.-J.; Wu, J.; Wang, K.-W.; Tang, Q.-L. Preparation and Sustained-Release Property of Triblock Copolymer/Calcium Phosphate Nanocomposite as Nanocarrier for Hydrophobic Drug. *Nanoscale Res. Lett.* **2010**, *5*, 781−785.

(57) Monfardini, C.; Veronese, F. M. Stabilization of Substances in Circulation. *Bioconjugate Chem.* **1998**, *9* (4), 418−450.

(58) George, A.; Shah, P. A.; Shrivastav, P. S. Natural Biodegradable Polymers Based Nano-Formulations for Drug Delivery: A Review. *Int. J. Pharm.* **2019**, *561*, 244−264.

(59) Kim, G. J.; Nie, S. Targeted Cancer Nanotherapy. *Mater. Today* **2005**, *8* (8), 28−33.

(60) Xiang, S. D.; Scholzen, A.; Minigo, G.; David, C.; Apostolopoulos, V.; Mottram, P. L.; Plebanski, M. Pathogen Recognition and Development of Particulate Vaccines: Does Size Matter? *Methods* **2006**, *40* (1), 1−9.

(61) Oyewumi, M. O.; Kumar, A.; Cui, Z. Nano-Microparticles as Immune Adjuvants: Correlating Particle Sizes and the Resultant Immune Responses. *Expert Rev. Vaccines* **2010**, *9* (9), 1095−1107.